JTTEE5 8:421-426

Alumina Coatings by Plasma Spraying of Monosize Sapphire Particles

L.C. Erickson, T. Troczynski, H.M. Hawthorne, H. Tai, and D. Ross

(Submitted 29 June 1998; in revised form 4 January 1999)

A series of plasma sprayed coatings of controlled microstructure was obtained by spraying three monosize sapphire powders using an axial injection torch in which the plasma gas composition and nozzle diameter were the only processing parameters varied. The effects of changes in these parameters on the coating splat morphology, porosity, angular crack distribution, and hardness are reported. The uniform, dense microstructure and the high hardness of 14 GPa (a level usually only associated with chromia thermal spray coatings) of the best alumina coatings resulted from using tightly controlled processing conditions and monodispersed precursor powders. The microstructural quality of plasma sprayed coatings and, hence, the coating properties can be improved significantly by minimizing variations in processing and raw material parameters.

Keywords alumina, microstructure, plasma spraying, wear

1. Introduction

Plasma sprayed coatings are used to improve the wear, thermal, electrical, and/or corrosion properties of machine components. It is important to understand the relation between deposition variables and coating quality. A large number of variables in the plasma spray process affects the quality and performance of the sprayed coatings. These include the choice of spray system, the various processing parameters (such as composition and flow rate of the plasma gas, the nozzle size of the plasma torch, and the torch-substrate standoff distance), and the choice of precursor powder, including the size range, shape, morphology, and composition of the particles.

The number of variables was reduced in this work by making the following choices. An axial injection plasma spray system was used to deposit a series of three very narrow size-range powders of high-purity single crystal alumina. Deposition was carried out in a nitrogen-base plasma with two levels of hydrogen content and two torch nozzle sizes to systematically vary the thermal and kinetic conditions for each of the three powder sizes.

The purpose of this work was to determine the effect of these few variables (i.e., particle size and relative heat input) on the characteristics of plasma sprayed coatings, such as microstructural integrity and the link to wear and mechanical properties, in an effort to optimize the performance of pure alumina coatings. Tribological and mechanical property aspects are presented elsewhere (Ref 1-4). This article focuses on the microstructural aspects of the coatings in order to examine the correlation between microstructural integrity and the coating deposition parameters.

This paper originally appeared in *Thermal Spray: Meeting the Challenges of the 21st Century; Proceedings of the 15th International Thermal Spray Conference,* C. Coddet, Ed., ASM International, Materials Park, OH, 1998. This proceedings paper has been extensively reviewed according to the editorial policy of the *Journal of Thermal Spray Technology.*

L.C. Erickson and **T. Troczynski,** Metals and Materials Engineering, University of BC, Vancouver, BC, Canada (Erickson is presently at Ballard Power Systems, Burnaby, B.C., Canada); **H.M. Hawthorne,** Tribology Group, National Research Council Canada, Vancouver, BC, Canada; and **H. Tai** and **D. Ross,** Northwest Mettech Corporation, Richmond, BC, Canada. Contact e-mail: lyneri@ballard.com.

2. Experimental Details

2.1 Materials

Coatings 250 to 350 μm thick were sprayed from 99.9% pure monocrystalline α-alumina powders nominally 5, 10, and 18 μm particle size (Sumicorundum AA-05, AA-10, and AA-18 powders, Sumitomo Chemical America, New York, NY) referred to later as AA5, AA10, and AA18 powders. Manufacturer's data indicate that these powders have a very narrow particle size distribution, with about 80 wt% lying between –20 and +30% of the specified size. These powders have a significantly more spherical morphology compared to the morphology of typical commercial powders (Fig. 1). The morphology, together with the narrow particle size distribution, helped to ensure uniform processing of all particles in the plasma. All coatings were sprayed onto mild steel substrates that had been grit blasted with alumina particles.

Coating specimens were prepared using an axial injection plasma spray system (Axial III plasma spray torch system, Northwest Mettech Corp.; Richmond, B.C., Canada). Some comparative data on radial injection sprayed (Plasmadyne plasma spray system) AA18 powder is also included and designated as conventional air plasma spray (APS) data. Two process parameters were varied from high and low values: between 10 and 20% hydrogen as a secondary plasma gas and between 12.5 and 14.1 mm orifice diameter of the plasma torch nozzle. Increasing the hydrogen concentration increases the thermal conductivity and heat content of the plasma jet. Increasing the nozzle size increases the powder residence time in the jet, while the smaller nozzle size causes the particles to travel faster through the jet, providing a higher impact velocity. At the high

values of both parameters, the powder particles are traveling more slowly through a hotter and more thermally conductive jet, allowing for more complete melting of the particles. Deposition of an ideal coating results from exposing the powder particles to an appropriate temperature for an adequate period of time. The matrix of processing conditions applied, along with their effect on heat input and particle residence time in the plasma, is summarized in Table 1.

Comparison of the processing conditions for the APS coatings that were sprayed by conventional radial injection plasma spray methods revealed that the relative heat input was low while the relative residence time was considered moderate.

2.2 Coating Characterization

Cross sections of the coatings were prepared by hot (60 °C) epoxy vacuum infiltration to preserve the true porosity. These infiltrated sections were then mounted and polished using standard metallographic techniques down to a final finish of 0.6 μm using a colloidal silica suspension.

The elemental and phase compositions of the coatings were obtained by x-ray powder diffractometry (XRD) using Cu Kα radiation. Coating microstructures were examined by optical microscopy and by secondary and backscattered electron (BSE) imaging in the scanning electron microscope (SEM).

Image analysis, using digital data from multiple BSE images (typically eight to ten per specimen on the outer $^2/_3$ of the coatings), provided quantitative estimates of the mean splat sizes, porosity, and angular crack distribution. The latter was measured according to the method described in Ref 5. As this method did not provide crack densities, vertical and horizontal crack densities were also determined using a simple grid method on the SEM micrographs. Scattered electron microscopy and BSE imaging were also used to characterize cross sections of coatings that had been fractured specifically to reveal their splat morphology. These were prepared by notching the substrate, cooling the specimens in liquid nitrogen, and breaking them with the coatings in tension. The surface roughness of the coatings was also measured by stylus profilometry (Talysurf 5, Rank Taylor-Hobson, Leicester, England).

Standard Vickers microhardness measurements were performed on cross-sectional surfaces at a load of 300 g, with 10 to 15 tests per sample. The wear properties of the coatings were evaluated using erosion and abrasion, along with scratch testing. The results can be used as a measure of microstructural integrity; that is, intersplat cohesion, in a plasma sprayed coating and are detailed elsewhere (Ref 1-4).

Table 1 Processing conditions

Spray run No.	H_2, vol%	Relative heat input	Torch nozzle size, mm	Relative residence time
1	10	Low	12.5	Less
2	10	Low	14.1	More
3	20	High	12.5	Less
4	20	High	14.1	More

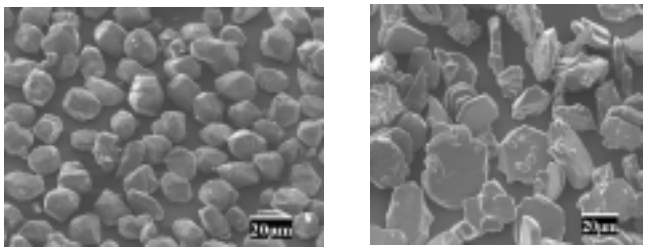

(a) (b)

Fig. 1 Alumina powders of types (a) 18 μm monocrystalline and (b) typical commercial (25-40 μm)

3. Results and Discussion

3.1 Microstructural Characterization

Microstructure and Phases. Overall views of the cross-sectional microstructures are shown in Fig. 2 for the low and high

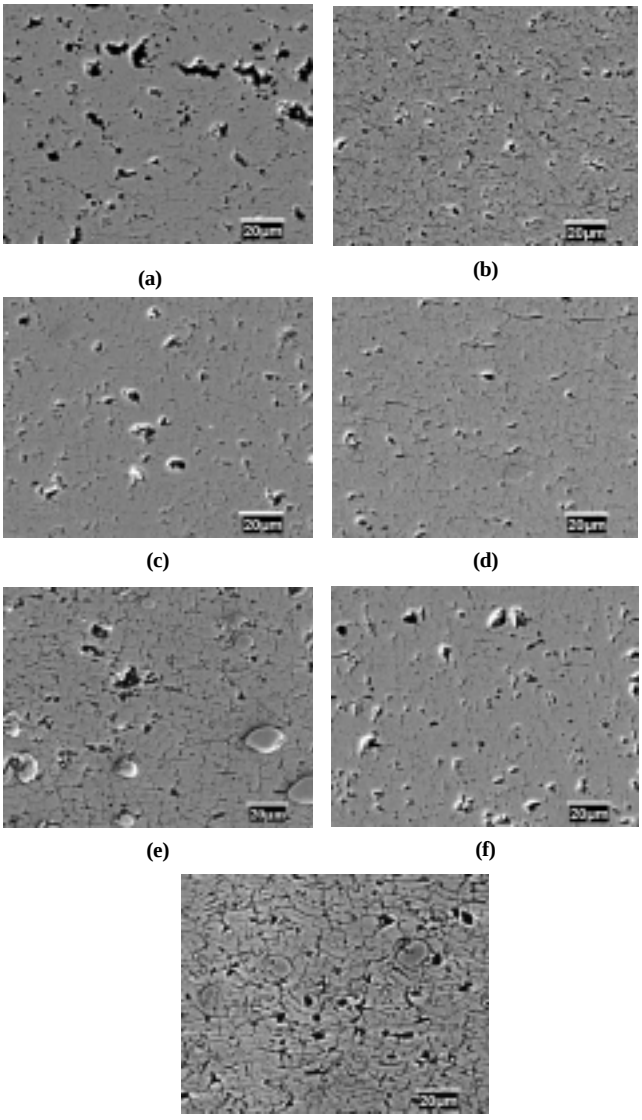

(a) (b) (c) (d) (e) (f) (g)

Fig. 2 Polished cross sections of the coatings. (a) AA5-1, (b) AA5-4, (c) AA10-1, (d) AA10-4, (e) AA18-1, (f) AA18-4, and (g) APS

heat input runs for each powder size. All of the coatings exhibited a decrease in visible porosity with increase in heat input and residence time. The AA5 coatings in particular appear to be most affected by the increase in heat input to the plasma. This is confirmed by the porosity data (Fig. 3) obtained from image analysis.

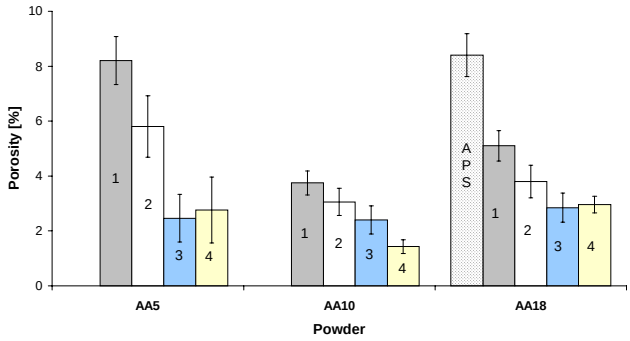

Fig. 3 Coating porosity from image analysis (8-10 images each), as a function of powder type and processing condition

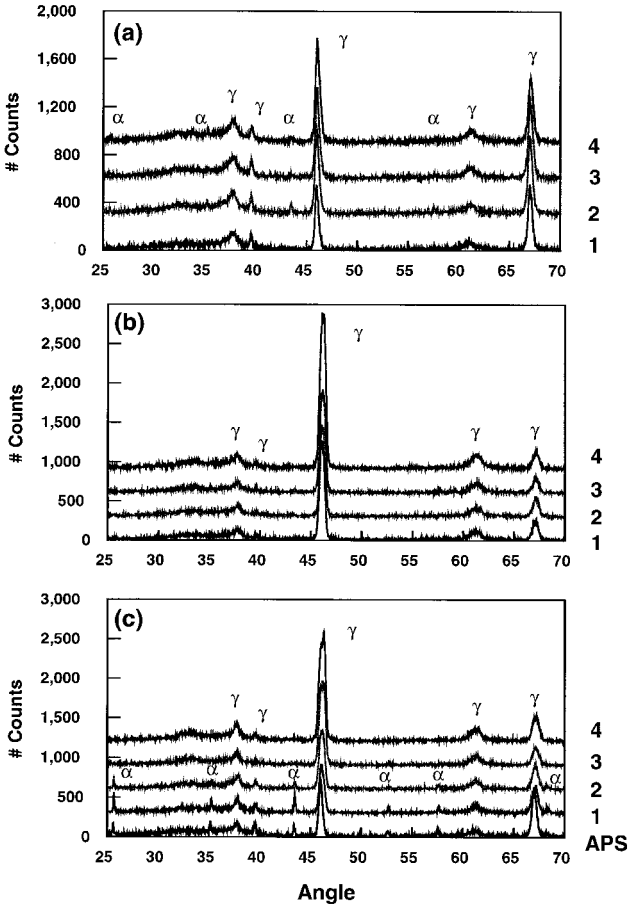

Fig. 4 X-ray powder diffraction spectra for the alumina coatings deposited in the four experiments. (a) AA5, (b) AA10, and (c) AA18 (includes the conventional plasma spray deposition of AA18 sapphire powder using a commercial radial powder injection system and labelled APS)

Each powder size was affected by the changes in processing conditions in a slightly different manner. The larger particles, AA18, were not completely melted during the lower heat input spray runs (No. 1, 2). This is evidenced by the unmelted particles visible in Fig. 2(e). However, the AA10 particles were completely molten during all four spray runs. These results were confirmed by XRD (Fig. 4), which shows that the as-deposited coatings consist mainly of γ-alumina. This is a result of rapid solidification of the molten precursor α-alumina particles. The amount of α-alumina present is indicative of the presence of unmelted and/or recrystallized particles in the coating (Ref 6).

Note the presence of the α-phase in the lower heat input processing conditions (run No. 1 and 2) for the larger AA18 particles, while none could be detected in the AA10 coatings. The AA5 particles are quite small, thus completely molten in the plasma. However, in run No. 2 to 4, with higher heat input and residence time, XRD detected a small amount of the α-phase present in these coatings (Fig. 4). It is theorized that this might be due to droplet splashing and subsequent recrystallization of submicron cusps of the molten particles.

Splat Morphology. The average measured splat diameter and pass thickness (i.e., the series of splats sprayed during each pass of the torch) for the different coatings is shown (Fig. 5). The largest difference observed is between the powder sizes. There is a trend within each powder series, from run No. 1 to 4, toward increased splat diameter and decreased relative pass thickness. These effects are visible on the top surface of coatings AA18-1

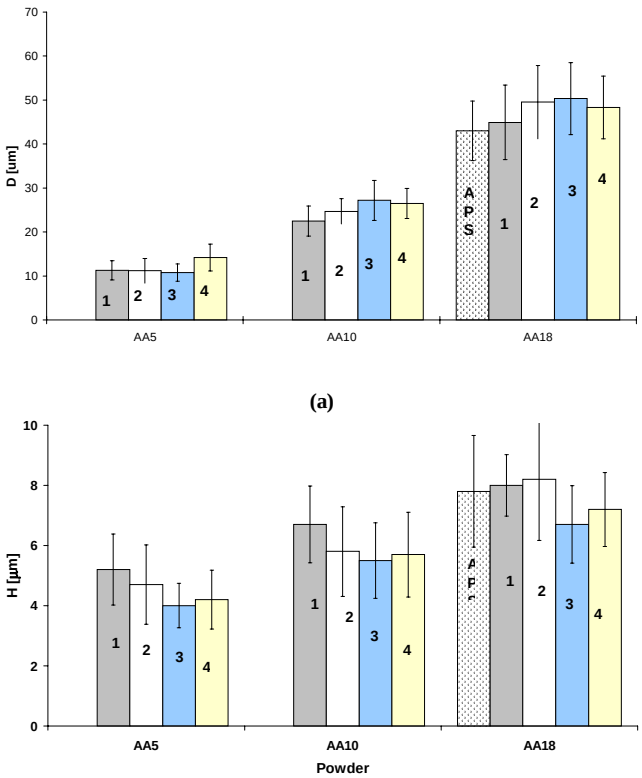

Fig. 5 Average dimensions of (a) splat diameter and (b) pass thickness, as a function of powder type and processing conditions

and AA18-4 in Fig. 6. Further discussion of the effect of this splat morphology on the wear of these coatings is presented elsewhere (Ref 1, 4). (Note that in Ref 1, an SEM marker bar problem, unknown at the time, led to the reporting of splat and pass dimensions that were too small by a factor of 1.667.)

The AA5 coatings (Fig. 6a) appeared to be porous and poorly consolidated, with no definite splat structure. The presence of numerous small particles was probably due to insufficient impact momentum. The AA10 coatings (Fig. 6b) exhibited the best splat morphology, with densely packed, overlapping (pancake-like) splats. The best AA18 coating (run No. 4) also showed a dense microstructure but with some evidence of breakup and flow at the splat edges. The surface morphology was also examined by measuring the surface roughness, R_a, values for each of the as-sprayed coatings (Fig. 7). Confirming the microstructural observations, Fig. 6, the AA5 coatings have the roughest surface with the AA10 coatings having the smoothest surface.

The average pass thickness was measured by detailed examination of fractured cross-sectional surfaces, examples of which are found in Fig. 8. It was difficult to measure the actual splat thicknesses due to the extent of grain growth through the splats, indicating improved intersplat cohesion, shown by the AA10 and AA18 coatings. Note the lack of a lamellar structure in the AA5 coating, however. The conventional APS coating also showed a less cohesive structure, indicating less than optimum processing of the sprayed particles.

Angular Crack Distribution. Comparison of the angular crack distribution for the different coatings provides an insight into some effects of the variations in processing conditions. A comparison of the ratio of horizontal (0 to 30°) to vertical (60 to 90°) cracks is given in Fig. 9. A graph of the average total cumulative length (in μm) versus the angle (0° is parallel to the substrate) for the three powder sizes is shown in Fig. 10. The cumulative lengths reflect the total length of the cracks and do not relate to the crack widths in any way.

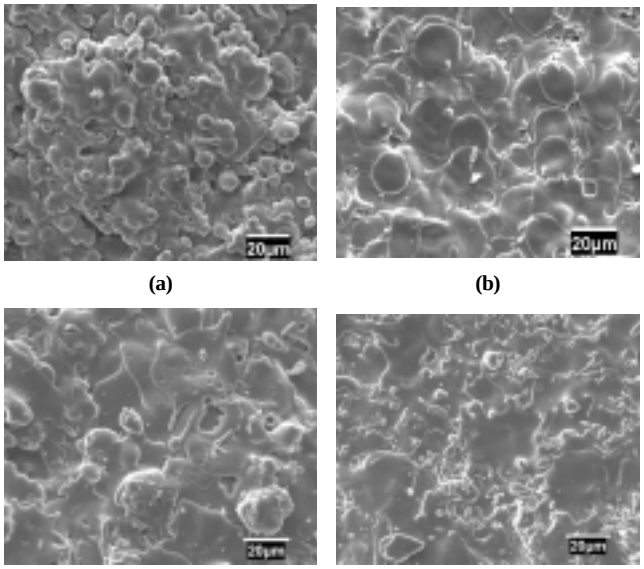

Fig. 6 Example of change in splat diameter with increased particle size, (a) AA5-4 and (b) AA10-4, and example of change in heat input, (c) AA18-1 and (d) AA18-4

The coatings produced from the 5 μm particles have a much higher ratio of horizontal to vertical cracks. This agrees with the structure observed on the fractured surfaces. There are a large number of horizontal delaminations along with minimal flattening of the splats. This is believed to be due to these particles having too little mass to achieve a sufficient impact velocity to produce a void-free coating. In contrast, the AA10 coatings all exhibited an evenly distributed crack network, while the larger AA18 coatings ranged from having a 1 to 1 ratio of horizontal to vertical cracks to having twice as many vertical cracks, as shown

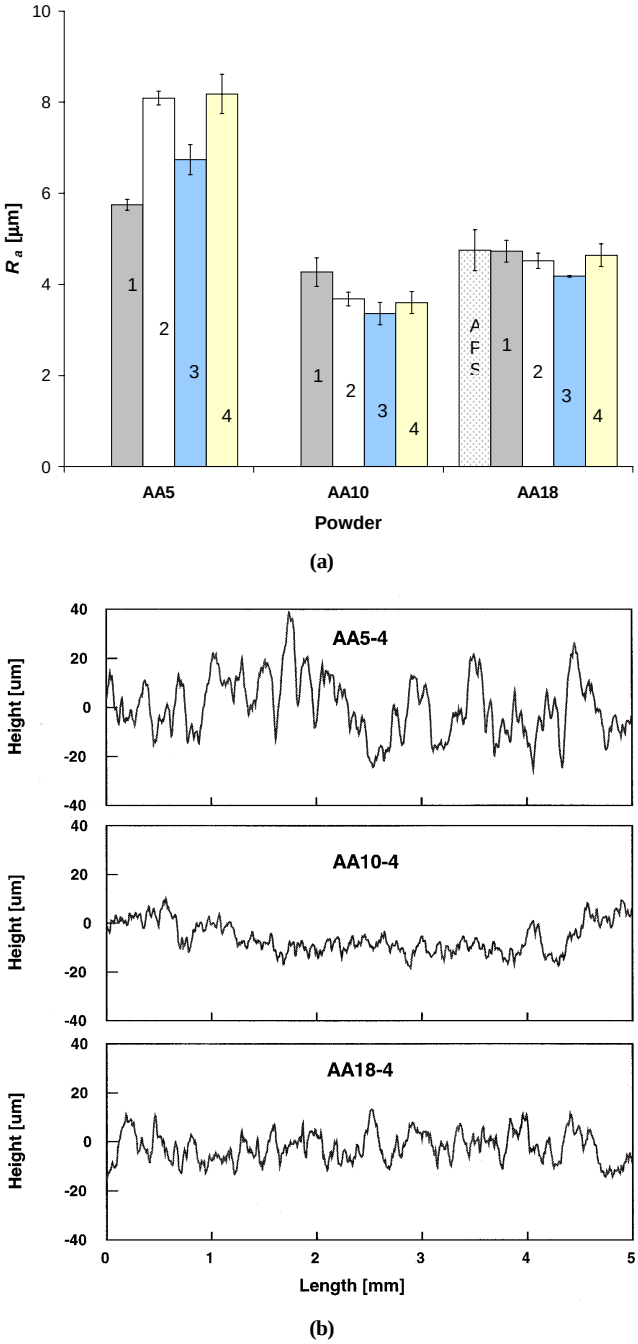

Fig. 7 Surface roughness (R_a values) of the coatings; (a) comparative graph and (b) typical roughness line scans

in Fig. 9. This can be a consequence of the greater intersplat cohesion of the larger particle derived coatings. As the splats were increasingly constrained or bonded along the horizontal direction, more vertical cracking occurred in the splats to accommodate the stresses due to solidification strain.

The measured densities of both vertical microcracks and horizontal delaminations for the coatings in the alumina matrix are shown in Fig. 11. Note that the AA5-4 coating contained roughly 2.5 times the vertical crack density of the other AA5 coatings, indicative of the increase in constraint of the particles as they solidified, which was caused by intersplat bonding. This is also visible in the increased vertical crack density seen in the AA10 and AA18 coatings. The APS and AA5 coatings contained the highest densities of horizontal delaminations, indicating poor intersplat bonding. The clearest trend toward decreased horizontal delaminations is shown by the AA18 series of coatings, while the vertical crack density remained basically constant.

3.2 *Mechanical and Wear Properties*

The microhardness results as measured on the cross-sectional surfaces are presented in Fig. 12. The general trend is again toward increased hardness as the heat input and time was increased. Coatings where the powders have not been melted thoroughly can exhibit either a higher hardness due to retained α-phase or a lower hardness due to poor interparticle bonding (cohesion). The maximum hardness values of 14 GPa are similar to those of plasma sprayed chromia coatings (Ref 7).

A number of different wear tests have been performed on the coatings to evaluate their microstructural integrity. These results

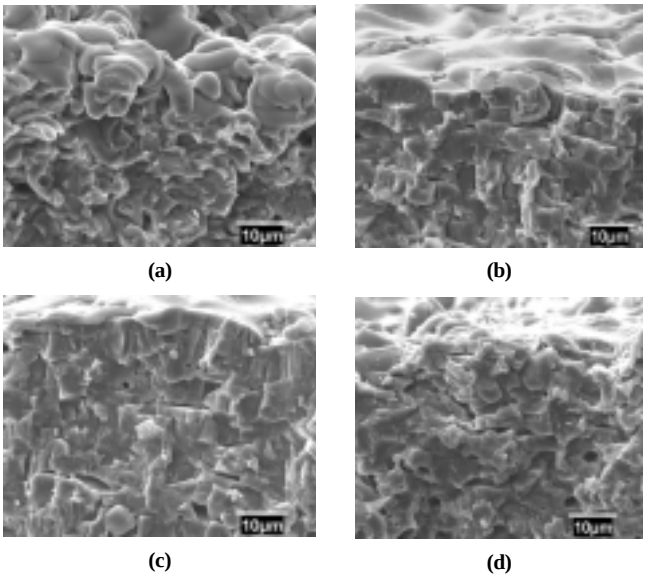

Fig. 8 Fracture/top surfaces: (a) AA5, (b) AA10, (c) AA18, and (d) APS (conventional air plasma spray) (radial injection sprayed AA18 powder)

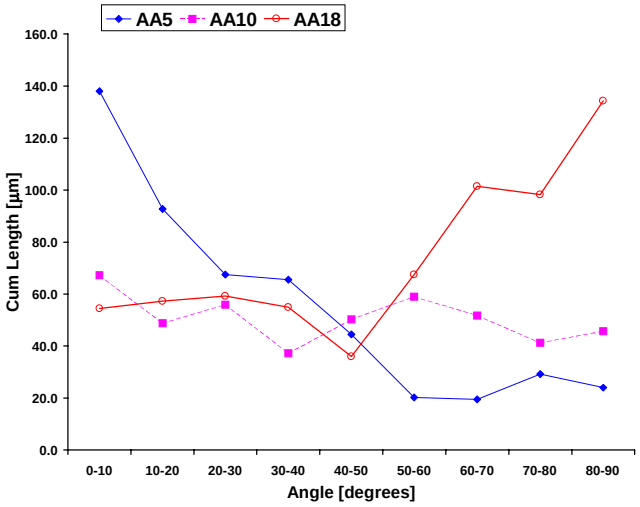

Fig. 10 Typical angular crack distribution for the three powder sizes (AA5-4, AA10-4, and AA18-4)

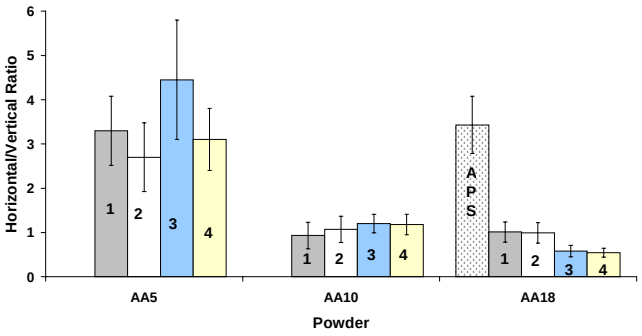

Fig. 9 The ratio of horizontal to vertical cracks for the different coatings as a function of powder type and processing conditions

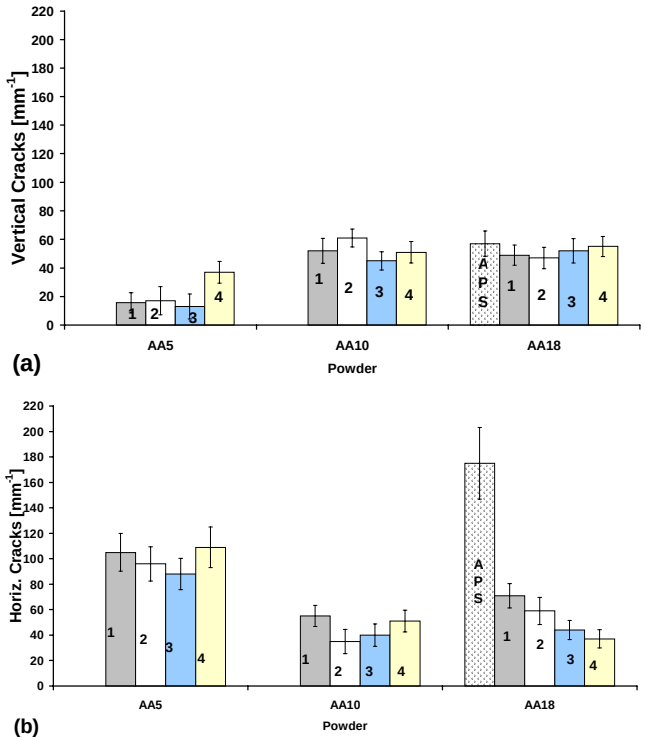

Fig. 11 Comparison of average crack densities (No./mm) for the coatings. (a) Vertical microcracks and (b) horizontal delaminations

are detailed elsewhere (Ref 1-4). Some correlations between the spray coating parameters, coating microstructure, and coating wear properties have been found, as illustrated by the abrasive wear results in Fig. 13. More detailed results and correlations are presented in Ref 4.

The coatings from the 5 and 18 μm powders showed improved wear resistance with an increase in heat input and residence time as compared to the 10 μm powder, which exhibited less sensitivity to variation in the processing conditions. The AA10 powder appears to be the optimum size for these spray conditions, as indicated by coatings with the lowest wear rate and greatest microstructural integrity.

3.3 *Effect of Parameter Changes on Microstructure and Coating Integrity*

The microstructural integrity of the coatings is dependent upon the intersplat bonding or cohesion. Cohesion is affected by the splat size, which is itself a function of the size of the precursor particles, along with the thermal conditions in the plasma. As seen in Fig. 5 and 6, the more flattened the splat appearance, the more intersplat bonding is likely to have occurred due to the impact momentum and heat input. This is evident in the growth of columnar grains through the splats in the AA10 and AA18 coatings as seen in the fracture surfaces in Fig. 7.

The angular crack distribution is also an indication of changes in the intersplat bonding or contact area. A change from less to more cohesive bonding between the splats results in the ratio of horizontal to vertical cracks going from a maximum with the finer particles (AA5) to a minimum with the larger (AA18). It is interesting to note that the coatings with an even distribution of both horizontal and vertical cracks also have the best microstructure and lowest porosity as well as the best wear and mechanical properties, as reported previously (Ref 1-4).

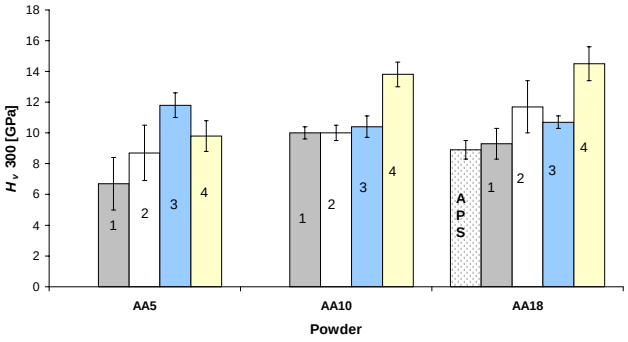

Fig. 12 Vickers microhardness (measured at 300 g load and expressed in GPa) on cross-sectional surfaces of the coatings

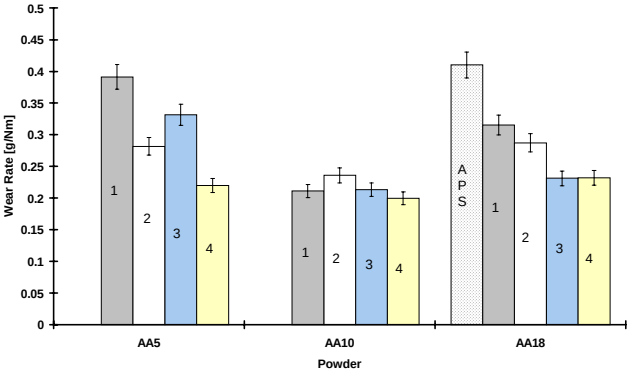

Fig. 13 Abrasive wear test results (block-on-drum using 200 μm, 80 grit SiC paper). Source: Ref 3

4. Conclusions

- The use of monodispersed powders and the axial injection plasma spray torch allows good control of the processing conditions experienced by the particles.
- Systematically varying the heat and momentum transfer efficiency (i.e., the precursor particle size, plasma thermal conductivity, and residence time of the particles in the plasma) provides a matrix of coatings with different microstructural integrity.
- The angular crack distribution is also an indication of changes in the intersplat bonding or contact area.
- Optimized particle size (10 μm particles) results in the best microstructural parameters (i.e., phase composition, porosity and splat structure) with the least sensitivity to variations in processing conditions.

Acknowledgment

Collaboration with researchers at Uppsala University, including R. Westergård, U. Wiklund, N. Axén, and S. Hogmark, particularly on some tribological aspects of this work, is acknowledged with gratitude. This research is supported by the National Science and Engineering Research Council (NSERC) of Canada.

References

1. H.M. Hawthorne, L.C. Erickson, D. Ross, H. Tai, and T. Troczynski, The Microstructural Dependence of Wear and Indentation Behavior of Some Alumina Plasma Sprayed Coatings, *Wear*, Vol 203-204, 1997, p 709-714
2. L.C. Erickson, R. Westergård, U. Wiklund, N. Axén, H.M. Hawthorne, and S. Hogmark, Cohesion in Plasma-Sprayed Coatings—A Comparison between Evaluation Methods, *Wear*, Vol 214, 1998, p 30-37
3. R. Westergård, L.C. Erickson, N. Axén, H.M. Hawthorne, and S. Hogmark, The Erosion and Abrasion Characteristics of Alumina Coatings Plasma Sprayed under Different Spraying Conditions, *Tribology Int.*, Vol 31, 1998, p 271-279
4. L.C. Erickson, "Wear and Microstructural Integrity of Ceramic Plasma Sprayed Coatings," Ph.D. dissertation, The University of British Columbia, Dept. of Metals and Materials Engineering, Vancouver, BC, 1998
5. M. Prystay, P. Gougeon, and C. Moreau, Correlation between Particle Temperature and Velocity and the Structure of Plasma Sprayed Zirconia Coatings, *Thermal Spray: Practical Solutions for Engineering Problems*, C.C. Berndt, Ed., ASM International, 1996, p 517-523
6. R. McPherson, The Relationship between the Mechanism of Formation, Microstructure and Properties of Plasma Sprayed Coatings, *J. Mater. Sci.*, Vol 15, 1980, p 3141-3149
7. G. Barbezat, A.R. Nicoll, and A. Sickinger, Abrasion, Erosion and Scuffing Resistance of Carbide and Oxide Ceramic Thermal Sprayed Coatings for Different Applications, *Wear*, Vol 162-164, 1993, p 529-537